

APLA: Additional Perturbation for Latent Noise with Adversarial Training Enables Consistency

Yupu Yao¹, Shangqi Deng¹, Zihan Cao¹, Harry Zhang², Liang-Jian Deng¹

¹University of Electronic Science and Technology of China, Chengdu, China

²Massachusetts Institute of Technology, Cambridge, USA

yypseek123@gmail.com, dengsq5856@126.com, dengsq5856@126.com, harryz@mit.edu, liangjian.deng@uestc.edu.cn

Abstract

Diffusion models have exhibited promising progress in video generation. However, they often struggle to retain consistent details within local regions across frames. One underlying cause is that traditional diffusion models approximate Gaussian noise distribution by utilizing predictive noise, without fully accounting for the impact of inherent information within the input itself. Additionally, these models emphasize the distinction between predictions and references, neglecting information intrinsic to the videos. To address this limitation, inspired by the self-attention mechanism, we propose a novel text-to-video (T2V) generation network structure based on diffusion models, dubbed Additional Perturbation for Latent noise with Adversarial training (APLA). Our approach only necessitates a single video as input and builds upon pre-trained stable diffusion networks. Notably, we introduce an additional compact network, known as the Video Generation Transformer (VGT). This auxiliary component is designed to extract perturbations from the inherent information contained within the input, thereby refining inconsistent pixels during temporal predictions. We leverage a hybrid architecture of transformers and convolutions to compensate for temporal intricacies, enhancing consistency between different frames within the video. Experiments demonstrate a noticeable improvement in the consistency of the generated videos both qualitatively and quantitatively.

Introduction

Generating video is a challenging task in computer vision, whose aim is to generate high-fidelity, diverse videos from various inputs like text, images, audio, or sketches. Recent works in deep learning have spurred considerable advancements in this domain, most notably through the advent of diffusion models (Ho, Jain, and Abbeel 2020). These models craft videos by iteratively introducing noise to an initial input, then undoing this noise through a series of denoising stages. Their strength is particularly notable in generating high-definition, extended-duration videos with intricate semantics and dynamics.

With the advancing capabilities of diffusion models, cross-modality generation tasks, including text-to-image (T2I) and text-to-video (T2V), have made substantial progress. Yet, the substantial data size of videos presents

Copyright © 2024, Association for the Advancement of Artificial Intelligence (www.aaai.org). All rights reserved.



(a) Tune-A-Video (Wu et al. 2022)



(b) APLA (Ours)

Figure 1: **The comparison (by the same prompt: “A man is skiing”) between Tune-A-Video and the proposed APLA.** (a) The result of Tune-A-Video is that the snowboard splits into multiple parts on these frames. (b) The obtained outcome is by our APLA method which keeps the single snowboard in all frames.

challenges in training video generation models from scratch. A recent approach, “Tune-A-Video” (Wu et al. 2022), aimed to utilize pre-trained T2I models for video synthesis. However, its outcomes exhibited inconsistencies across video frames. Ensuring frame consistency in video generation, especially within fine-tuned models, remains a hurdle. While some efforts have achieved acceptable frame consistency using diffusion models (Höppe et al. 2022), intricate video details, especially in complex scenarios, are often absent. For instance, even with identical prompts and inputs, the “Tune-A-Video” approach still manifests inconsistencies in generated videos. Moreover, extending fine-tuning epochs could potentially compromise the semantic coherence between successive frames.

In light of these challenges, we propose a novel architecture, *i.e.*, APLA. Using self-attention (Vaswani and Shazeer 2023), APLA is geared to capture inherent video characteristics and establish connections between frames by adaptively generating parameters. To facilitate efficient information extraction from inputs, we devise a much smaller model compared to diffusion models, as shown in the success of style transfer and multi-task learning (Zhang and Agrawala 2023). The result can be observed visually in Fig. 2. Consequently, we engineer a decoder-only structure for our Video Generation Transformer (VGT). With masking and self-attention mechanisms, VGT exhibits an improvement in predicting



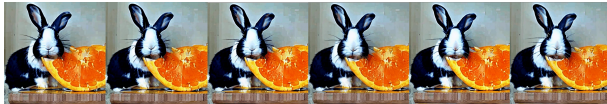
(a) An SUV is moving on the road, cartoon style



(b) An SUV is moving on the beach



(c) A puppy is eating an orange



(d) A rabbit is eating an orange

Figure 2: Visual demonstrations of APLA using different prompts.

unknown frames, demonstrating its ability to distill intrinsic input information. We also introduce a novel loss function, hyper-loss, to encourage the model to focus on nuanced input details. Lastly, to further enhance the generated quality of video and improve the consistency between different frames, we introduce adversarial training to improve the quality of output while strengthening the robustness. The contributions of this work can be summarized as follows:

1. A novel architecture, *i.e.*, VGT, builds on top of pre-trained diffusion models, which enhances the consistency between video frames by learning the correlation information between input frames.
2. A fusion of the diffusion model and adversarial is employed for video generation, where adversarial training is directly applied to the discrepancy in noise distributions, rather than judging the similarity between input and output images.
3. Quantitative and qualitative experiments that demonstrate the effectiveness of the proposed approach, which achieves SOTA performance in frame consistency of generated videos.

Related Work

Cross-Modal Video Generation

Generating videos using multiple input modalities presents a formidable challenge within the realm of deep learning. A particularly prominent endeavor in video generation is the synthesis of videos through text-to-video (T2V) techniques, which entails creating videos grounded in natural language descriptions. This innovative synthesis process can be conceptualized as an evolution beyond the established domain

of text-to-image (T2I) synthesis. In a broader context, models for text-to-image (T2I) synthesis can be systematically categorized into two distinctive classes: transformer-based models and diffusion-based models. The former category, as exemplified by references such as (Ramesh et al. 2021; Sim et al. 2019; Zhang 2016), leverages the power of extensively trained large-scale language models such as GPT-3 or T5. These models adeptly transform textual input into latent vectors, which are subsequently employed for downstream image generation. Conversely, the latter category represented by models like (Nichol et al. 2022; Zhang et al. 2020, 2021), also incorporates a text encoder in a similar vein, yet diverges in their approach by integrating the text-encoded information into the diffusion process. The prowess of diffusion-based models in crafting intricate images stands evident. This capability has been the foundation for their evolution from text-to-image (T2I) synthesis to the more dynamic realm of text-to-video (T2V) synthesis. However, these initial methods had shortcomings like detail deficiency, temporal inconsistencies, and limited control. Recent approaches have emerged to address these issues and enhance text-to-video (T2V) synthesis.

Diffusion Model

The inception of the Denoising Diffusion Probabilistic Model (DDPM), documented in (Ho, Jain, and Abbeel 2020), took inspiration from thermodynamic frameworks. This model, functioning as a Markov chain, exhibits an auto-encoder structure. Nevertheless, its inference process faced sluggishness owing to the intricate denoising stages encompassed. To address this issue, Denoising Diffusion Implicit Models (DDIM)(Song, Meng, and Ermon 2020) introduced an innovative strategy: by introducing variable variance for predicted noise, they achieved swift inference for the diffusion model within a concise span of steps. Building upon the foundations laid by DDIM, subsequent endeavors (Watson et al. 2022; Zhang, Eisner, and Held 2023) aimed to propel DDPM inference to even greater speeds.

Broadly speaking, the Diffusion model’s key strength lies in its remarkable capacity for handling tasks involving cross-modality and multi-modality interactions. This strength is vividly demonstrated by the Latent Diffusion Model (LDM) (Rombach et al. 2022; Pan et al. 2023; Eisner, Zhang, and Held 2022), which not only exhibited the potential of diffusion for high-resolution image generation through the utilization of latent spaces but also showcased the model’s ability to excel in cross-modality scenarios. The application of the Diffusion model to video generation has prompted various approaches (Ho et al. 2022; Lim et al. 2021, 2022; Avigal, Paradis, and Zhang 2020; Avigal et al. 2021). Among these, Tune-A-Video (Wu et al. 2022; Devgon et al. 2020; Shen et al. 2024; Jin et al. 2024) stands out for introducing a novel perspective on video generation via diffusion modeling. This innovative methodology views video generation as a process of refining a pre-trained stable diffusion. In doing so, Tune-A-Video reshapes our understanding of how diffusion models can be harnessed to address the challenges of video generation with a fresh and effective approach.

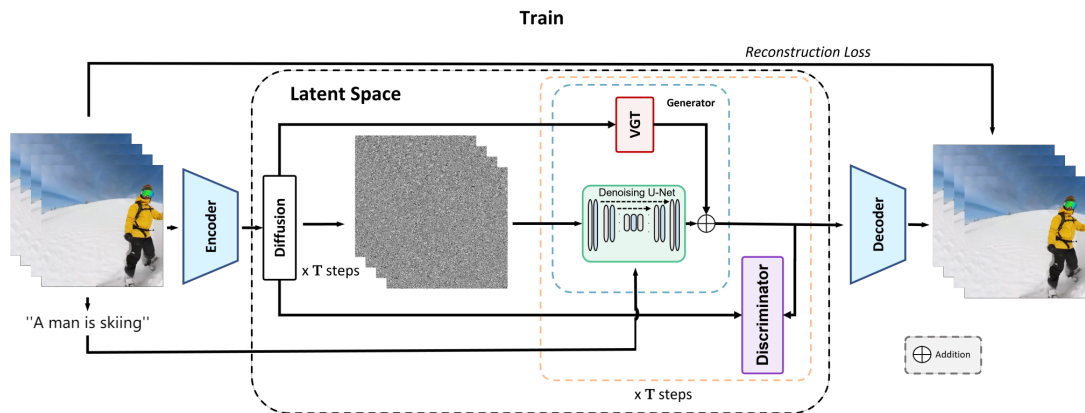


Figure 3: **The process of training the networks.** VGT extracts intrinsic information from latent variables, considering various time steps for noise incorporation, and especially including the clean latent variable devoid of noise, namely the original latent variable z . As VGT is not trained ever, the output of VGT is tiny thus the change of the output is small, which is helpful to improve the consistency of different frames without changing the content a lot. The discriminator receives the predicted noise and the noise residuals for corresponding time steps in the diffusion stage.

Methodology

In this section, we begin by presenting the overall structure of APLA. Subsequently, we delve into the details of VGT, designed to extract intrinsic information. Notably, we introduce two versions of VGT, each showcasing distinct advantages in the experiment. Following this, we discuss hyper-loss and introduce our adversarial training strategy.

APLA

To enhance inter-frame consistency, alongside optimizing high-quality outputs, it’s imperative to account for the inter-connections among distinct frames. While prior research assumed that inherent information could be naturally grasped by the model without supplementary steps, the challenge becomes more pronounced in complex tasks like video generation, where depicting high-level temporal features during inference proves more intricate compared to image generation. In light of this, we introduce a novel architecture (depicted in Fig. 3) that builds upon the diffusion model and integrates an additional module. This module is specifically designed to capture intrinsic information and foster inter-frame connections within the temporal domain. This approach sets us apart from previous methods and addresses the nuances presented by video generation. A visual comparison between APLA and Tune-A-Video is illustrated in Fig. 1. Specifically, the added module incorporates a self-attention mechanism aimed at extracting information directly from inputs, all without introducing any additional loss. Our hypothesis is rooted in the potential of self-attention mechanisms to gather relevant details from the input itself. This implies the ability to dynamically generate parameters based on input, empowering the model with strong inductive capabilities.

To ensure content consistency with the introduced module, we propose that the module’s output should manifest as subtle perturbations, significantly smaller in magnitude than the output of the pre-trained model (referred to as U-Net in

Algorithm 1: Additional Perturbation for Latent Noise with Adversarial Training (APLA)

Input: A text query q , a reference video v , a pre-trained T2I diffusion model with encoder ε and decoder \mathcal{D} , a number of iterations T , VGT φ , a discriminator D

Output: A generated video \hat{x} that matches the text query

Initialize \hat{x} as an empty list

Extract the first frame x_0 from v

Encode x_0 and q into a latent code z_0 using DDIM inversion

for $t = 1$ to T **do**

 Compute z_{t+1} through Eq. 1

 Fine-tune the model parameters θ of ε using Eq. 20

end for

for $t = T, T - 1, \dots, 1$ **do**

 Sampling \hat{z}_{t-1} using DDIM inversion

if $t == 1$ **then**

 Obtain $\hat{x} = \mathcal{D}(\hat{z}_t)$

end if

end for

return \hat{x}

this paper). The evolving ratio of perturbation to U-Net output over epochs can be visually observed in Fig. 5(b). Let the input be denoted as $x \in \mathbb{R}^{B \times H \times W \times F \times C}$, where B , H , W , F , and C represent batch, height, width, frame, and channel dimensions respectively. We define the encoder as \mathcal{E} , decoder as \mathcal{D} , and $\hat{x} = \mathcal{D}(z) = \mathcal{D}(\mathcal{E}(x))$ signifies the intended outcome. Furthermore, considering the process in the latent space, let Z denote the latent space with $z \in Z$, where $z \in \mathbb{R}^{B \times h \times w \times F \times c}$, where h , w , c are the dimension in the latent space respectively. The diffusion process and U-Net are represented by ϕ and π respectively. The term z_T in the denoising stage signifies the latent variable’s evolution over T steps with added noise. A pivotal addition is our

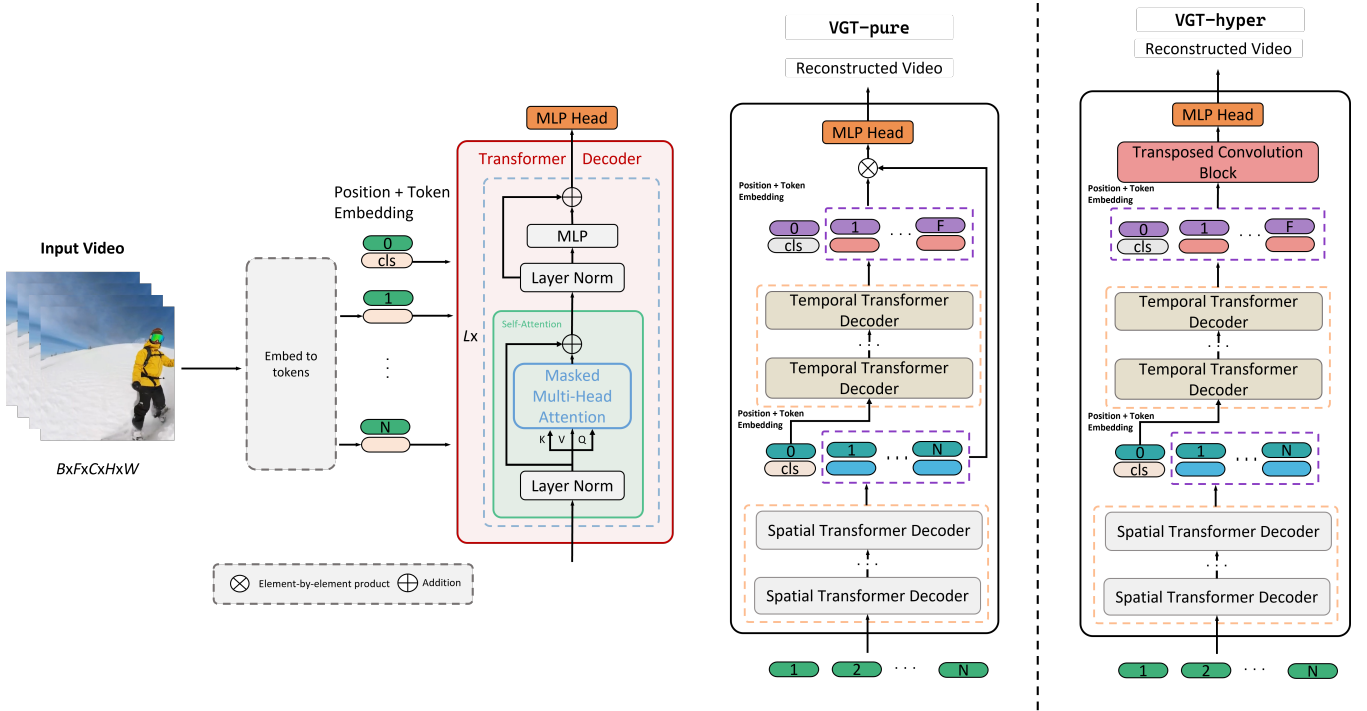


Figure 4: **An illustration of VGT-Pure and VGT-Hyper.** The left side shows the transformer decoder structure, which adapted mask operation on the self-attention mechanism especially. The right side shows the two versions of VGT. The Temporal Transformer Decoder only receives the class (*i.e.*, *cls*) token of output sequences of the Spatial Transformer Decoder. The rest of the tokens of the output of the Spatial Transformer Decoder are used to multiply with the tokens of the Temporal Transformer Decoder output dislodging *cls* token in VGT-Pure, while the whole output of the Temporal Transformer Decoder is transmitted to Transposed Convolution Block directly in VGT-Hyper.

module, termed Video Generation Transformer (VGT). Denoted as φ , it encapsulates an abstract function. The series of denoising autoencoders is represented as $\epsilon_\theta(x_t, t)$, with $t = 1, \dots, T$, where t corresponds to the specific step in the sequence. Then, we have

$$z_t = \phi(z_{t-1}, t - 1), \quad (1)$$

$$\hat{z}_{T-1} = \pi(z_T, T). \quad (2)$$

$$\hat{z}_{t-1} = \pi(\hat{z}_t, t), \quad (3)$$

where \hat{z}_t represents the predicted output of denoising U-Net at the t -th step. In fact, we add the perturbation to the U-Net, which aims to capture intrinsic information:

$$\hat{z}_{t-1}^* = \pi(\hat{z}_t, t) + \varphi(z_t, t), \quad (4)$$

thus the original object function:

$$\mathcal{L}_{MSE} := \mathbb{E}_{\mathcal{E}(x), \epsilon \sim \mathcal{N}(0,1), t} \left[\|\epsilon - \epsilon_\theta(\hat{z}_t, t)\|_2^2 \right], \quad (5)$$

can be rewritten as:

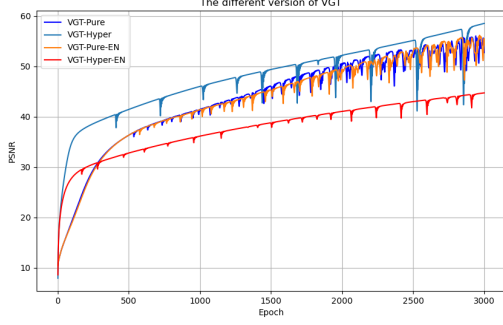
$$\mathcal{L}_{MSE} := \mathbb{E}_{\mathcal{E}(x), \epsilon \sim \mathcal{N}(0,1), t} \left[\|\epsilon - \epsilon_\theta(\hat{z}_t^*, t)\|_2^2 \right]. \quad (6)$$

For clarity, the intuitive pseudocode is illustrated in the Algorithm 1. With the adversarial training that enhances the robustness and quality of the generator output, a discriminator is set to receive the predicted noise and noise residuals in the corresponding step. More elaborate discussions are presented in the following sections.

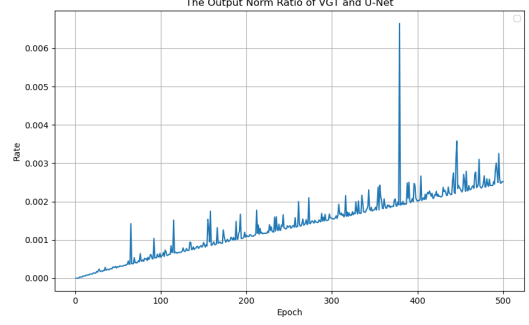
Video Generation Transformer (VGT)

We introduce the proposed VGT, designed as a decoder-only architecture. With self-attention mechanisms, this Transformer efficiently focuses on input features. Compared to pure encoder-based structures like BERT (Devlin et al. 2019), the pure Transformer decoder architecture (Liu et al. 2018) accommodates more tokens, boosting its processing capacity. The design of the decoder within the Transformer stands out as a unique case in the realm of autoregressive models (Dai and Le 2015), showcasing potential in unsupervised time series prediction (Brown, Mann et al. 2020). Besides, this design empowers the Transformer decoder to extract temporal information from input data. For tasks involving time sequences, the self-attention mechanisms of the Transformer decoder enhance output distribution coherence by extracting contextual insights. Notably, even with incomplete sequence inputs, Transformer decoders promote model diversity (Esser, Rombach, and Ommer 2021), thereby bolstering generalization capabilities.

Nonetheless, in previous video generation models employing Transformer architectures, like Video Transformer (VIVIT) (Arnab et al. 2021), solely the Transformer encoder is utilized to derive a latent variable. This variable is subsequently fed into another network, often a classifier, to fulfill the downstream task. Consequently, VIVIT lacks the direct capability to generate videos. It is precisely due to this



(a) Comparison of VGT versions



(b) Ratio of VGT output and U-Net

Figure 5: (a) is the comparison of different versions of VGT. “EN” represents the use of a transformer encoder instead of a decoder, which means the mask operation was not included. As the picture shows, VGT-Hyper performs the best while the encoder version of VGT-Hyper performs the worst. For VGT-Pure, the encoder version performs similarly to the decoder version, while the performance of the two versions is between VGT-Hyper and VGT-Hyper-EN. (b) shows the ratio of VGT output and U-Net in the denoising step. The result shows that the norm of VGT output is very tiny compared with the U-Net output, which shows that the output of VGT did not change the original output much while improving the consistency of different frames laterally.

| VGT version | | |
|--------------|---------------|----------------------|
| Version | PSNR | Trainable Parameters |
| VGT-Pure | 52.746 | 60.362M |
| VGT-Hyper | 58.552 | 97.136M |
| VGT-Pure-EN | 54.236 | 60.362M |
| VGT-Hyper-EN | 42.736 | 97.136M |

Table 1: The different version of VGT, while “EN” represents the transformer encoder to be used instead of the encoder, which means there is no mask operation. We compare the PSNR of the reconstruction quality, as the input is the single video generated randomly. Meanwhile, we compare the trainable parameters of different VGT, while the VGT-Pure and VGT-Pure-EN own the lowest trainable parameters, for the mask operation did not change the quantities of trainable parameters.

limitation that we introduce the Video Generation Transformer (VGT). Our framework aims to reconstruct or generate videos, leading to the proposal of two distinct VGT variants. The first is a pure Transformer decoder approach, referred to as VGT-pure, while the second combines self-attention with 3D convolution, termed VGT-Hyper.

VGT-Pure

The initial model variant is a pure Transformer decoder. We denote the input sequence in the ℓ_{th} layer as \mathbf{z}_s^ℓ and \mathbf{z}_t^ℓ , where s and t stand for spatial and temporal aspects respectively. Furthermore, we define a token as $\mathbf{z}_{cls,s}^{k,\ell}$, with “cl” signifying the class token, and k representing the k -th token in the sequence, excluding the class token. In this context, we replace Multi-Headed Self Attention (MAS) with MASKed Multi-Headed Self Attention (MMAS). Likewise, each transformer

block encompasses layer normalization (LN). The spatial decoder block can be succinctly represented as follows:

$$\mathbf{z}_s^{\ell+1} = \text{MMSA}(\text{LN}(\mathbf{z}_s^\ell)) + \mathbf{z}_s^\ell, \quad (7)$$

and similarly the temporal decoder block as:

$$\mathbf{z}_t^{\ell+1} = \text{MMSA}(\text{LN}(\mathbf{z}_t^\ell)) + \mathbf{z}_t^\ell. \quad (8)$$

We consider L layers of spatial decoder at all, and the \mathbf{z}_t^L can be represented as:

$$\mathbf{z}_s^L = [\mathbf{z}_{cls,s}^L, \mathbf{z}_s^{1,L}, \mathbf{z}_s^{2,L}, \dots, \mathbf{z}_s^{F,L}] + \mathbf{p}, \quad (9)$$

where \mathbf{p} denotes the positional embedding, and \mathbf{z} is divided into tokens. Among these tokens, the first one is $\mathbf{z}_{cls,s} \in \mathbb{R}^{F \times (H_{patch} \times W_{patch}) \times L}$, serving as a compact feature commonly used for categorical embedding. Here, H_{patch} represents the patch’s height, and W_{patch} is the width of a patch. When we split $\mathbf{z}_{cls,s}$ along the temporal frame dimension, we obtain individual tokens $\mathbf{z}_{cls,s}^{1,L}, \mathbf{z}_{cls,s}^{2,L}, \dots, \mathbf{z}_{cls,s}^{F,L}$, where $\mathbf{z}_{cls,s}^{i,L} \in \mathbb{R}^{1 \times (H_{patch} \times W_{patch}) \times L}$ for $i = 1, 2, \dots, F$. Simultaneously, we maintain the collection $[\mathbf{z}_s^{1,L}, \mathbf{z}_s^{2,L}, \dots, \mathbf{z}_s^{F,L}]$ as $\mathbf{z}_s^{C,L}$, facilitating skip connections. This arrangement leads us to use $\mathbf{z}_{cls,s}^L$ as the input for the temporal decoder, setting it apart from the rest. This ultimately yields the expression for \mathbf{z}_t^1 :

$$\mathbf{z}_t^1 = [\mathbf{z}_{cls,t}^1, \mathbf{D}\mathbf{z}_{cls,s}^{1,L}, \mathbf{D}\mathbf{z}_{cls,s}^{2,L}, \dots, \mathbf{D}\mathbf{z}_{cls,s}^{F,L}] + \mathbf{p}, \quad (10)$$

where \mathbf{D} is the decoder block. Suppose we have M layers temporal decoder in total. Similarly, the output of M_{th} can be written as:

$$\mathbf{z}_t^M = [\mathbf{z}_{cls,t}^M, \mathbf{z}_{cls,t}^{1,M}, \mathbf{z}_{cls,t}^{2,M}, \dots, \mathbf{z}_{cls,t}^{F,M}] + \mathbf{p}, \quad (11)$$

| Frame Consistency | | | | |
|---|--------------|------------|--------------|---------------|
| Method | CLIP Score | FVD | IS | FCI |
| CogVideo (Hong et al. 2022) | 90.64 | 626 | 50.46 | 0.2942 |
| Plug-and-Play (Tumanyan et al. 2022) | 88.89 | - | - | 0.3048 |
| VideoGPT (Yan et al. 2021) | 47.12 | - | 24.69 | 0.4567 |
| DVD-GAN (Clark, Donahue, and Simonyan 2019) | 48.36 | - | 27.38 | 0.4012 |
| TGANv2 (Saito et al. 2020) | 51.26 | 1209 | 28.87 | 0.3538 |
| MoCoGAN-HD (Tian, Ren, and Chai 2021) | 77.64 | 838 | 32.36 | 0.3156 |
| DIGAN (Yu and Tack 2022) | 81.26 | 655 | 29.71 | 0.3012 |
| TATS-base (Ge and Hayes 2022) | 90.65 | 332 | 79.28 | 0.2647 |
| Tune-A-Video (Wu et al. 2022) | 92.40 | 864 | 64.12 | 0.2716 |
| SAVE (Karim et al. 2023) | 94.81 | - | - | 0.2628 |
| APLA (Ours) | 96.21 | 512 | 71.26 | 0.2576 |

Table 2: Quantitative comparison with evaluated baselines by measuring content consistency with text prompt using CLIP Score (\uparrow), FVD (\downarrow), IS (\uparrow) and FCI (\downarrow), which measures how many users prefer each model. FCI (\downarrow) is the metric that computes the optical flow difference of the adjacent frame. The lower, the better.

Similarly, we denote $[\mathbf{z}_{cls,t}^{1,M}, \mathbf{z}_{cls,t}^{2,M}, \dots, \mathbf{z}_{cls,t}^{F,M}]$ as $\mathbf{z}_t^{C,M}$, then the output of VGT-Pure can be written as:

$$\mathbf{y} = \mathbf{z}_s^{C,L} \odot \mathbf{z}_t^{C,M}, \quad (12)$$

$$\hat{\mathbf{z}}_t = \text{MLP}(\mathbf{y}), \quad (13)$$

where \odot represents the Hadamard product, MLP represents multilayer perceptron and t is t -th step. we get $\hat{\mathbf{z}}_t \in \mathbb{R}^{B \times F \times (H_{patch} \times W_{patch}) \times (C \times P \times P)}$, then we rearrange the $\hat{\mathbf{z}}_t$ into $\varphi(z_t)$, where $\varphi(z_t) \in \mathbb{R}^{B \times F \times C \times (H_{patch} \times P) \times (W_{patch} \times P)}$ and $\varphi(\cdot)$ is the function representation of VGT-Pure while z_t is the input of VGT-Pure, and $(H_{patch} \times P) = H$ and $(W_{patch} \times P) = H$.

VGT-Hyper

In this section, we introduce the second variant of VGT, named VGT-Hyper, which leverages 3D convolution (Tran et al. 2015). Particularly, in Eq. 12, rather than employing element-wise multiplication, we opt for 3D convolution. We represent the convolution block with the matrix \mathbf{M} , leading to the following expression:

$$\mathbf{y}^* = \mathbf{M}\mathbf{z}_t^M, \quad (14)$$

$$\hat{\mathbf{z}}_t = \text{MLP}(\mathbf{y}^*). \quad (15)$$

Unlike VGT-pure, VGT-Hyper demonstrates superior performance in the reconstruction task, as indicated in Tab. 1, all the while maintaining a higher number of trainable parameters. VGT-Hyper capitalizes on the benefits inherent in a transformer decoder, underscoring the efficacy of the mask operation for time series tasks, depicted in Fig. 5(a).

Hyper-Loss for Latent Noise Fitting

Recognizing the limitations of Mean Squared Error (MSE) for certain generative tasks (Zhang et al. 2018), we introduce a novel loss function tailored for video generation. We adopt a perceptual loss approach within the diffusion model, akin to prior studies (Lugmayr et al. 2022). In detail, we formalize ℓ_1 loss and perceptual loss separately as follows:

$$\mathcal{L}_{L1} := \mathbb{E}_{\mathcal{E}(x), \epsilon \sim \mathcal{N}(0,1), t} [\|\epsilon - \epsilon_\theta(z_t^*, t)\|_1], \quad (16)$$

and

$$\mathcal{L}_{per} := \mathbb{E}_{\mathcal{E}(x), \epsilon \sim \mathcal{N}(0,1), t} [dist_{per}(\epsilon, \epsilon_\theta(z_t^*, t))]. \quad (17)$$

Expanding upon this, we incorporate a hyper-loss that encompasses the weighted combination of Mean Squared Error (MSE), ℓ_1 loss, and perceptual loss. The ℓ_1 loss serves as a regularization term to promote sparsity in the solution, while the perceptual loss encourages the model to generate more photorealistic images. This concept is illustrated as follows:

$$\mathcal{L}_{hyper} := \alpha * \mathcal{L}_{MSE} + \beta * \mathcal{L}_{L1} + \gamma * \mathcal{L}_{per}, \quad (18)$$

where α , β and γ represent the weights.

Adversarial Training with 1×1 Convolution

In our approach, we view adversarial training as a valuable form of regularization. For video generation, the distinction between integrating Generative Adversarial Networks (GANs) and employing perceptual loss lies in their treatment of temporal information. Perceptual loss is primarily concerned with the structural attributes of individual frames, whereas reconstruction loss focuses on pixel-level closeness. In contrast, GAN loss centers around maintaining consistency across frames, promoting temporal coherence. Besides, it is important to recognize that GANs have a propensity for capturing global information by treating all frames holistically. This approach leads to an enhancement in video quality through adversarial training. The discriminator, in the APLA, receives the output of the generator, namely the predicted noise to compare with the noise residual, which is obtained in the diffusion process. More concretely, the diffusion process T steps, while the denoising process aims to inverse this process, which predicts the noise residual, the difference of the t -th step and $t-1$ -th step, namely the adding noise. In the denoising process, for instance, the generator predicts the t -th step noise residual, and then the discriminator receives the corresponding t -th step noise in the diffusion process, aiming to decline the distance of two noise distributions (noise residual and predicted noise residual).

| Frame Consistency | | | | |
|------------------------------|--------------|---------------|--------------------------|-------------------|
| Method | CLIP Score | FCI | CLIP Score (1500 epochs) | FCI (1500 epochs) |
| Full Model (ours) | 96.21 | 0.2764 | 96.76 | 0.2470 |
| w/o Discriminator | 94.42 | 0.2714 | 93.70 | 0.2178 |
| w/o VGT&Discriminator | 91.44 | 0.1918 | 96.13 | 0.2655 |
| w/o Hyper-Loss&Discriminator | 93.97 | 0.2476 | 93.06 | 0.2588 |
| w/o VGT&Hyper-Loss | 94.83 | 0.2534 | 96.38 | 0.2172 |

Table 3: Ablation studies on APLA’s different components. Compared via CLIP score and FCI on each model variation trained with 750 epochs(default) and 1500 epochs respectively.

The proposed discriminator structure is streamlined, comprising only a 1×1 convolutional layer. This kernel comprehensively considers frame positional data, aiding temporal similarity extraction. Denoting the discriminator as $D(\cdot)$ and with $x \sim p(x)$, we arrive at a min-max problem:

$$\max_D \min_G \mathbb{E}_{x \sim p(x)} [\log D_G^*(x)] + \mathbb{E}_{x \sim p_g} [\log (1 - D_G^*(x))], \quad (19)$$

where G represents the generator, which is the united block of U-Net and VGT in this paper, while D represents the discriminator. Let the fusion loss of the generator, in this paper, which is the fusion of U-Net and VGT, as L_g , where $L_g = \mathbb{E}_{x \sim p(x)} [\log D_G^*(x)] + \mathbb{E}_{x \sim p_g} [\log (1 - D_G^*(x))]$. Hence, the final optimization objective is

$$\min_{\theta} \max_G \mathcal{L}_{hyper} + \lambda L_g, \quad (20)$$

where λ is a coefficient to adjust the performance and θ is the parameters of the network.

Experiments

Implementation Details

We build the model based on Tune-A-Video (Wu et al. 2022; Elmquist et al. 2022) and utilize the pre-trained weights of the Stable Diffusion (Rombach et al. 2022). We uniformly sample 24 frames at a resolution of 512×512 from the input video and train the models for 750 steps and 1500 steps with a learning rate of $3e-5$ and a batch size of 1. For the hyperparameter induced by loss, we set α of 0.5, β of 0.2, γ of 0.1, and λ of 0.5. Due to the limited CUDA memory, we chose the VGT-pure only for the following experiment. During inference, we employ the DDIM sampler (Song, Meng, and Ermon 2020) with classifier-free guidance (Ho and Salimans 2022) in our experiments. For a single video, it takes about 90 minutes for 1500 steps and approximately 1 minute (while Tune-A-Video takes 60 minutes) for sampling on an NVIDIA 3090 GPU.

Dataset: To evaluate our approach, we use representative videos taken from the DAVIS dataset (Pont-Tuset et al. 2017). During fine-tuning, we just train the model on a single video. The video descriptions and captions automatically used an off-the-shelf captioning model (Li et al. 2023), which is regarded as the default prompt of our video.

Qualitative Results: A visual comparison is presented between our approach and the baseline in Fig. 1(a), focusing on reconstructing tasks using the same prompt. We observe that Tune-A-Video does not reconstruct the details

in each frame well. Specifically, the sled visibly splits into two pieces in some frames. Our model provides more stable and smooth results compared with the Tune-A-Video. Also, readers can find more results obtained by our method in Fig. 2.

Quantitative Results: Quantitative assessment is conducted, as depicted in Tab. 2. Regarding content consistency, we evaluate the CLIP score (Radford et al. 2021) across all generated frames by employing average cosine measurements. This metric serves as an indicator of the semantic coherence within the generated videos. In terms of frame consistency, we employ the flow consistency index (FCI) for comparison. Unlike (Varghese et al. 2020), we directly compute the flow field between consecutive frames, independent of the input video. Specifically, we determine the optical flow field between two adjacent frames, assess alterations in the local optical flow field concerning each pixel’s value and its domain, and subsequently average all the computed changes. The results underscore that, in comparison to our baseline model, enhancements are observed in both content consistency and frame consistency.

Ablation Studies

We conduct ablation studies to assess the importance of different components of ALVA, as shown in Tab. 3. The proposed full APLA model performs the best considering content consistency and frame consistency together. Without some components, APLA’s performance degrades but still performs better than Tune-A-Video. We also discuss the influence of the number of epochs. From observing Tab. 3, we see that with the epoch increasing, the quantitative score is increasing. However, from the visual result, we see that too many epochs can cause overfitting, which destroys the result influenced by the prompt. Without the Discriminator, as the number of epochs increases, it is easy to fall into local minima which decreases the CLIP score and FCI. For w/o VGT&Discriminator, although the final FCI is decent, it cannot retain the semantic consistency and needs too many epochs to reach a good result. For w/o Hyper-Loss&Discriminator, the single VGT can just reach a normal level and it is hard for it to approach a better score because of the limitation of convergence. As w/o VGT&Hyper-Loss, the model performance is close to w/o Discriminator and even better. However, it still needs too many epochs to reach such a good result.

Conclusion

In this study, we introduce APLA, which includes a compact module for capturing intrinsic or temporal information, and the novel VGT architecture, a pure transformer decoder similar to GPT. To fortify the robustness and quality of our APLA model, we employ adversarial training during its training process. Through experiments, our model achieves state-of-the-art performance in video reconstruction and videos from textual prompts (T2V).

References

- Arnab, A.; Dehghani, M.; Heigold, G.; Sun, C.; Lučić, M.; and Schmid, C. 2021. Vivit: A video vision transformer. In *ICCV*, 6836–6846.
- Avigal, Y.; Paradis, S.; and Zhang, H. 2020. 6-DoF grasp planning using fast 3D reconstruction and grasp quality CNN. *arXiv preprint arXiv:2009.08618*.
- Avigal, Y.; Satish, V.; Tam, Z.; Huang, H.; Zhang, H.; Danielczuk, M.; Ichnowski, J.; and Goldberg, K. 2021. Avplug: Approach vector planning for uncontact grasping amid clutter. In *2021 IEEE 17th international conference on automation science and engineering (CASE)*, 1140–1147. IEEE.
- Brown, T. B.; Mann, B.; et al. 2020. Language Models are Few-Shot Learners. *arXiv:2005.14165*.
- Clark, A.; Donahue, J.; and Simonyan, K. 2019. Adversarial Video Generation on Complex Datasets. *arXiv:1907.06571*.
- Dai, A. M.; and Le, Q. V. 2015. Semi-supervised Sequence Learning. *arXiv:1511.01432*.
- Devgon, S.; Ichnowski, J.; Balakrishna, A.; Zhang, H.; and Goldberg, K. 2020. Orienting novel 3D objects using self-supervised learning of rotation transforms. In *2020 IEEE 16th International Conference on Automation Science and Engineering (CASE)*, 1453–1460. IEEE.
- Devlin, J.; Chang, M.-W.; Lee, K.; and Toutanova, K. 2019. BERT: Pre-training of Deep Bidirectional Transformers for Language Understanding. *arXiv:1810.04805*.
- Eisner, B.; Zhang, H.; and Held, D. 2022. Flowbot3d: Learning 3d articulation flow to manipulate articulated objects. *arXiv preprint arXiv:2205.04382*.
- Elmqvist, A.; Young, A.; Hansen, T.; Ashokkumar, S.; Caldararu, S.; Dashora, A.; Mahajan, I.; Zhang, H.; Fang, L.; Shen, H.; et al. 2022. ART/ATK: A research platform for assessing and mitigating the sim-to-real gap in robotics and autonomous vehicle engineering. *arXiv preprint arXiv:2211.04886*.
- Esser, P.; Rombach, R.; and Ommer, B. 2021. Taming transformers for high-resolution image synthesis. In *CVPR*, 12873–12883.
- Ge, S.; and Hayes, T. 2022. Long Video Generation with Time-Agnostic VQGAN and Time-Sensitive Transformer. *arXiv:2204.03638*.
- Ho, J.; Chan, W.; Saharia, C.; Whang, J.; Gao, R.; Gritsenko, A.; Kingma, D. P.; Poole, B.; Norouzi, M.; Fleet, D. J.; et al. 2022. Imagen video: High definition video generation with diffusion models. *arXiv*.
- Ho, J.; Jain, A.; and Abbeel, P. 2020. Denoising diffusion probabilistic models. *NeurIPS*, 33: 6840–6851.
- Ho, J.; and Salimans, T. 2022. Classifier-free diffusion guidance. *arXiv*.
- Hong, W.; Ding, M.; Zheng, W.; Liu, X.; and Tang, J. 2022. CogVideo: Large-scale Pretraining for Text-to-Video Generation via Transformers. *arXiv:2205.15868*.
- Höppe, T.; Mehrjou, A.; Bauer, S.; Nielsen, D.; and Dittadi, A. 2022. Diffusion models for video prediction and infilling. *arXiv*.
- Jin, D.; Karmalkar, S.; Zhang, H.; and Carlone, L. 2024. Multi-Model 3D Registration: Finding Multiple Moving Objects in Cluttered Point Clouds. *arXiv preprint arXiv:2402.10865*.
- Karim, N.; Khalid, U.; Joneidi, M.; Chen, C.; and Rahnavard, N. 2023. SAVE: Spectral-Shift-Aware Adaptation of Image Diffusion Models for Text-guided Video Editing. *arXiv:2305.18670*.
- Li, J.; Li, D.; Savarese, S.; and Hoi, S. 2023. Blip-2: Bootstrapping language-image pre-training with frozen image encoders and large language models. *arXiv*.
- Lim, V.; Huang, H.; Chen, L. Y.; Wang, J.; Ichnowski, J.; Seita, D.; Laskey, M.; and Goldberg, K. 2021. Planar robot casting with real2sim2real self-supervised learning. *arXiv preprint arXiv:2111.04814*.
- Lim, V.; Huang, H.; Chen, L. Y.; Wang, J.; Ichnowski, J.; Seita, D.; Laskey, M.; and Goldberg, K. 2022. Real2sim2real: Self-supervised learning of physical single-step dynamic actions for planar robot casting. In *2022 International Conference on Robotics and Automation (ICRA)*, 8282–8289. IEEE.
- Liu, P. J.; Saleh, M.; Pot, E.; Goodrich, B.; Sepassi, R.; Kaiser, L.; and Shazeer, N. 2018. Generating Wikipedia by Summarizing Long Sequences. *arXiv:1801.10198*.
- Lugmayr, A.; Danelljan, M.; Romero, A.; Yu, F.; Timofte, R.; and Van Gool, L. 2022. RePaint: Inpainting Using Denoising Diffusion Probabilistic Models. In *CVPR*, 11461–11471.
- Nichol, A.; Dhariwal, P.; Ramesh, A.; Shyam, P.; Mishkin, P.; McGrew, B.; Sutskever, I.; and Chen, M. 2022. GLIDE: Towards Photorealistic Image Generation and Editing with Text-Guided Diffusion Models. *arXiv:2112.10741*.
- Pan, C.; Okorn, B.; Zhang, H.; Eisner, B.; and Held, D. 2023. Tax-pose: Task-specific cross-pose estimation for robot manipulation. In *Conference on Robot Learning*, 1783–1792. PMLR.
- Pont-Tuset, J.; Perazzi, F.; Caelles, S.; Arbeláez, P.; Sorkine-Hornung, A.; and Van Gool, L. 2017. The 2017 davis challenge on video object segmentation. *arXiv*.
- Radford, A.; Kim, J. W.; Hallacy, C.; Ramesh, A.; Goh, G.; Agarwal, S.; Sastry, G.; Askell, A.; Mishkin, P.; Clark, J.; et al. 2021. Learning transferable visual models from natural language supervision. In *ICML*, 8748–8763. PMLR.
- Ramesh, A.; Pavlov, M.; Goh, G.; Gray, S.; Voss, C.; Radford, A.; Chen, M.; and Sutskever, I. 2021. Zero-Shot Text-to-Image Generation. *arXiv:2102.12092*.

- Rombach, R.; Blattmann, A.; Lorenz, D.; Esser, P.; and Ommer, B. 2022. High-resolution image synthesis with latent diffusion models. In *CVPR*, 10684–10695.
- Saito, M.; Saito, S.; Koyama, M.; and Kobayashi, S. 2020. Train Sparsely, Generate Densely: Memory-Efficient Unsupervised Training of High-Resolution Temporal GAN. *IJCV*, 128(10-11): 2586–2606.
- Shen, S.; Zhu, Z.; Fan, L.; Zhang, H.; and Wu, X. 2024. Diff-CLIP: Leveraging Stable Diffusion for Language Grounded 3D Classification. In *Proceedings of the IEEE/CVF Winter Conference on Applications of Computer Vision*, 3596–3605.
- Sim, K. C.; Beaufays, F.; Benard, A.; Guliani, D.; Kabel, A.; Khare, N.; Lucassen, T.; Zadrazil, P.; Zhang, H.; Johnson, L.; et al. 2019. Personalization of end-to-end speech recognition on mobile devices for named entities. In *2019 IEEE Automatic Speech Recognition and Understanding Workshop (ASRU)*, 23–30. IEEE.
- Song, J.; Meng, C.; and Ermon, S. 2020. Denoising diffusion implicit models. *arXiv*.
- Tian, Y.; Ren, J.; and Chai, M. 2021. A Good Image Generator Is What You Need for High-Resolution Video Synthesis. *arXiv:2104.15069*.
- Tran, D.; Bourdev, L.; Fergus, R.; Torresani, L.; and Paluri, M. 2015. Learning Spatiotemporal Features with 3D Convolutional Networks. *arXiv:1412.0767*.
- Tumanyan, N.; Geyer, M.; Bagon, S.; and Dekel, T. 2022. Plug-and-Play Diffusion Features for Text-Driven Image-to-Image Translation. *arXiv:2211.12572*.
- Varghese, S.; Bayzidi, Y.; Bär, A.; Kapoor, N.; Lahiri, S.; Schneider, J. D.; Schmidt, N.; Schlicht, P.; Hüger, F.; and Fingscheidt, T. 2020. Unsupervised Temporal Consistency Metric for Video Segmentation in Highly-Automated Driving. In *CVPRW*, 1369–1378.
- Vaswani, A.; and Shazeer, N. 2023. Attention Is All You Need. *arXiv:1706.03762*.
- Watson, D.; Chan, W.; Ho, J.; and Norouzi, M. 2022. Learning Fast Samplers for Diffusion Models by Differentiating Through Sample Quality. In *ICLR*.
- Wu, J. Z.; Ge, Y.; Wang, X.; Lei, W.; Gu, Y.; Hsu, W.; Shan, Y.; Qie, X.; and Shou, M. Z. 2022. Tune-A-Video: One-Shot Tuning of Image Diffusion Models for Text-to-Video Generation. *arXiv*.
- Yan, W.; Zhang, Y.; Abbeel, P.; and Srinivas, A. 2021. VideoGPT: Video Generation using VQ-VAE and Transformers. *arXiv:2104.10157*.
- Yu, S.; and Tack, J. 2022. Generating Videos with Dynamics-aware Implicit Generative Adversarial Networks. *arXiv:2202.10571*.
- Zhang, H. 2016. Health diagnosis based on analysis of data captured by wearable technology devices. *International Journal of Advanced Science and Technology*, 95: 89–96.
- Zhang, H.; Eisner, B.; and Held, D. 2023. Flowbot++: Learning generalized articulated objects manipulation via articulation projection. *arXiv preprint arXiv:2306.12893*.
- Zhang, H.; Ichnowski, J.; Avigal, Y.; Gonzales, J.; Stoica, I.; and Goldberg, K. 2020. Dex-Net AR: Distributed deep grasp planning using a commodity cellphone and augmented reality app. In *2020 IEEE International Conference on Robotics and Automation (ICRA)*, 552–558. IEEE.
- Zhang, H.; Ichnowski, J.; Seita, D.; Wang, J.; Huang, H.; and Goldberg, K. 2021. Robots of the lost arc: Self-supervised learning to dynamically manipulate fixed-endpoint cables. In *2021 IEEE International Conference on Robotics and Automation (ICRA)*, 4560–4567. IEEE.
- Zhang, L.; and Agrawala, M. 2023. Adding conditional control to text-to-image diffusion models. *arXiv*.
- Zhang, R.; Isola, P.; Efros, A. A.; Shechtman, E.; and Wang, O. 2018. The Unreasonable Effectiveness of Deep Features as a Perceptual Metric. *arXiv:1801.03924*.